Evaluation of impacts of cooling tower design properties on the near-field environment

CrossMark

Jaiho Lee*

Advanced Reactor Development Lab., Korea Hydro & Nuclear Power Co., Ltd., Central Research Institute, Republic of Korea

ABSTRACT

In a nuclear power plant, ultimate heat sink (UHS) and circulating water system (CWS) cooling towers both ultimately remove heat from the essential service water system, main condenser, and non-essential service water system during all operation modes including accident conditions. Since the visible plume from the cooling tower has an adverse effect on the environment, however, an environmental impact assessment of the cooling tower is required for the construction of a new nuclear power plant. In this study, the environmental impact of UHS and CWS cooling towers of an APR1400 standard design plant was assessed for the purpose of testing and demonstrating the recently-updated SACTI2 model. Because the site for the APR1400 standard design plant had not been decided, one-year meteorological data from the Spokane International Airport weather station, WA, USA, were used as hypothetical input data for the environmental impact assessment. The quantitative effect of cooling tower design changes on the environment was analyzed in terms of index-value dispersion area (A_D) and dispersion ratio (δ) for nine environmental assessment indexes. Scenario test conditions were varied by changing cooling tower arrangement, distance between cooling towers, length of cooling tower, exit port height, exit port diameter, the number of exit ports, heat load per tower, and air flow rate per tower.

1. Introduction

Since 1980, in the United States, closed-cycle cooling design such as in cooling towers has been applied to most new nuclear power plants on account of environmental regulations and policies relating to the effect of the increased temperature of discharged water on the environment, the impact of the cooling intake structures on underwater organisms, and fresh water availability (EPRI, 2012). However, plumes from cooling towers can generate adverse impacts on the environment such as through plume shadowing, water and salt deposition, ground level fogging and icing, and solar energy loss, among others (Davis, 1998; U.S. NRC, 2007). The environmental impact of cooling towers operating on the plant site can be investigated by measurement devices placed near the cooling tower region. On the other hand, the evaluation of the environmental impact of a cooling tower under construction or to be constructed in the future should be conducted through experiment or numerical analysis based on past meteorological information. Full-scale experiments for predicting the dynamic behavior of cooling tower plumes are expensive; scale model experiments (Michioka et al., 2007; Ruiz et al., 2016) have their limitations; therefore, many studies (Carhart and Policastro, 1991; Carhart et al., 1992; Orville et al., 1980;

Moore, 1977) on the environmental impact of cooling towers have focused on developing an analytical plume prediction model. Policastro et al. (1981a) developed an improved mathematical model, more well-known as the seasonal/annual cooling tower impact (SACTI) model, for predicting plume and drift behavior occurring from cooling towers. They also developed a user manual of the improved mathematical model (Policastro et al., 1984) and updated it in terms of user friendliness (Dunn et al., 1987). The single plume behavior using the SACTI model was tested and validated with data from the Chalk Point Dye Tracer Study (Policastro et al., 1981a). The behavior of multiple plumes using the SACTI model was also validated against the multiple unit cooling towers at Pittsburgh, CA (Policastro et al., 1981b). The original SACTI code has been available in public domain and accepted by both the United States Environmental Protection Agency (U.S. EPA) and the United States Nuclear Regulatory Commission (U.S. NRC) (EPRI, 2015).

Due to recent advances in computational fluid dynamics (CFD) techniques, studies (Lucas et al., 2010; Meroney, 2008; Chahine et al., 2015; Milosavljevic and Heikkilä, 2001) have been carried out to apply CFD techniques to the environmental assessment of a cooling tower, yielding predictions of more detailed accurate plume behaviors. Nevertheless, the SACTI model has been popular due to its low cost for

Nomenclature

A_D	index-value dispersion area
n	number of radial locations from the starting point of the coordinate system
m	number of the wind rose direction used in the model
N_i	number of i_{th} subsector in the j_{th} location
S_j	the area of subsector
A_0	the region-of-interest area

Greek symbols

δ	dispersion ratio ($\delta = A_D/A_0$)

$\delta_{Test}/\delta_{Test-1}$	normalized dispersion ratio

Subscript

Test	test scenario
i	wind rose direction index
j	radial location index
0	region-of-interest
D	dispersion

the analysis and conservative results for licensing; therefore, it has been widely used in developing environmental reports required for combined construction and operation licensing application (COLA) of nuclear power plants (Wan, 2007; U.S. NRC, 2011; U.S. NRC, 2013; U.S. NRC, 2008). Due to that reason, EPRI (Electric Power Research Institute) developed an upgraded SACTI2 model for new nuclear power plant construction (EPRI, 2015). For the real testing of the updated SACTI2 model, in the present study, environmental assessment of ultimate heat sink (UHS) and circulating water system (CWS) cooling towers of an APR1400 (for Advanced Power Reactor 1400 MW electricity) for the application of U.S. NRC standard design certification were numerically carried out for a hypothetical plant site: Spokane International Airport station (WBAN No.: 24157 and USAF No.: 727850) from the national weather service (NWS). Most nuclear power plants in the U.S. are located in the central and eastern U.S. which are in humid climates. However, SACTI2 user's manual used one year meteorological data for Spokane International Airport providing sufficiently cold condition to investigate the effect of plume-induced fogging and icing due to cooling towers.

For the air quality modeling analysis, the U.S. EPA recommends to use five-year data of a site of interest so that the data covers the wide spectrum of the meteorological conditions for the site (U.S. EPA, 2005). One year meteorological data might be not enough to fully address meteorological conditions for the environmental assessment of the site of interest because of a wide variability of meteorological conditions from year to year. In this study, however, the same one year meteorological data for Spokane International airport used in SACTI2 user's

manual (EPRI, 2015) was applied for the environmental assessment of cooling towers of the APR1400 standard plant because the site for APR1400 has not been determined yet.

The main objective of this study is to quantify the effect of cooling tower design changes of APR1400 standard design plant on the environment using SACTI2 model. Several test conditions were applied to investigate the effect of cooling tower design changes on the near-field environment of the plant. The results were analyzed using environmental assessment indexes: plume length frequency (PLF), plume shadowing hour (PSH), plume fogging hour (PFH), plume icing hour (PIH), plume salt deposition flux (PSDF), plume water deposition flux (PWDF), fractional solar energy deposition loss (FSDL), fractional beam deposition loss (FBDL), and total solar energy loss (TSL).

2. Methodology

2.1. Cooling tower design

The main cooling system of pressurized water reactor (PWR) nuclear power plants consists of safety-related UHS and non-safety-related CWS. The UHS is responsible for finally removing reactor residual heat and essential station heat loads during all modes of operation including accident conditions. The key safety functions of the UHS are to dissipate residual heat after normal shutdown and an accident such as a LOCA (loss-of-coolant-accident), and the expected maximum decay heat from the spent fuel pool (NRC RG 1.27, 2015). On the other hand, the CWS provides cooling water to dissipate heat from the main condenser and
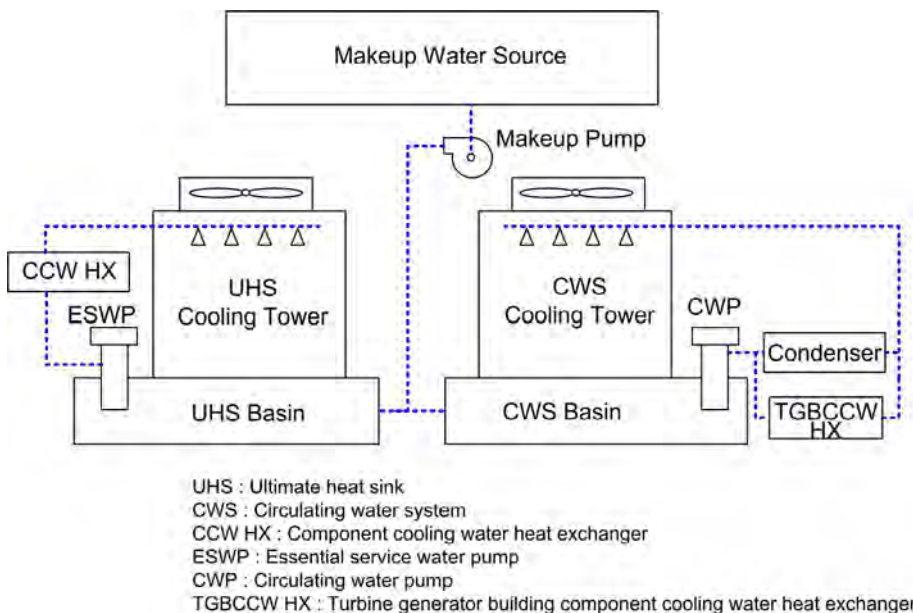

Fig. 1. Simplified diagram of water flows in circulating water system (CWS) and ultimate heat sink (UHS).

UHS : Ultimate heat sink
CWS : Circulating water system
CCW HX : Component cooling water heat exchanger
ESWP : Essential service water pump
CWP : Circulating water pump
TGBCCW HX : Turbine generator building component cooling water heat exchanger

non-essential service water system. Based on the specific site characteristics of the plant, the cooling system is designed as either a once-through cooling or a closed-cycle cooling system (EPRI, 2012). Located on the shores of a sea, lake, or wide-river, the plant draws water from a source water body with a large enough amount of water to eject plant heat loads, and returns it back to the same body of water, referred to as once-through cooling. In inland sites without a large body of water, cooling towers with the concept of a closed-cycle cooling system are used as the cooling system to dissipate heat to the atmosphere by evaporation. The UHS and CWS of the APR1400 standard design plant were designed as wet-type mechanical draft counterflow cooling towers (U.S. NRC, 2014a,b). Fig. 1 shows a schematic diagram of the heat dissipation process through the UHS and CWS cooling towers of the APR1400 standard design plant. The blue dashed lines represent flows of water in the cooling system. UHS cooling towers remove heat from the essential service water system (ESWS) by providing cooling water to the component cooling water heat exchanger (CCW HX), whereas the circulating water cooling towers supply cooling water to the main condenser and turbine generator building open cooling water system (TGBOCWS) to dissipate heat from the turbine generator building component cooling water heat exchanger (TGBCCW HX).

In general, cooling towers are designed with site-specific data based on meteorological information for the past several years. When it comes to the available area for installing cooling towers on the plant site, a detailed cooling tower design including general arrangement and layout, exit port size, fan size, and basin size is optimized at the stage of construction. At the stage of design certification, however, a conceptual design of the cooling towers is conducted with the design input data enveloping all sites of the United States because site-specific meteorological data are not available (U.S. NRC, 2014c). Table 1 lists the design parameters of CWS and UHS cooling towers of an APR1400 standard design plant. The safety-related UHS was designed considering the concept of two divisions, consisting of two cooling towers per division, three cells per cooling tower, and one electric fan per cell. Three cells in a UHS cooling tower were designed to support a capacity of 33 $\frac{1}{3}$% each for operating a tower at 100% capacity. During almost all modes of operation, including normal, startup, shutdown, refueling, abnormal operations and accident conditions, one cooling tower in each UHS division operates. Meanwhile, the non-safety-related CWS, consisting of two cooling towers and 28 cells per cooling tower, operates
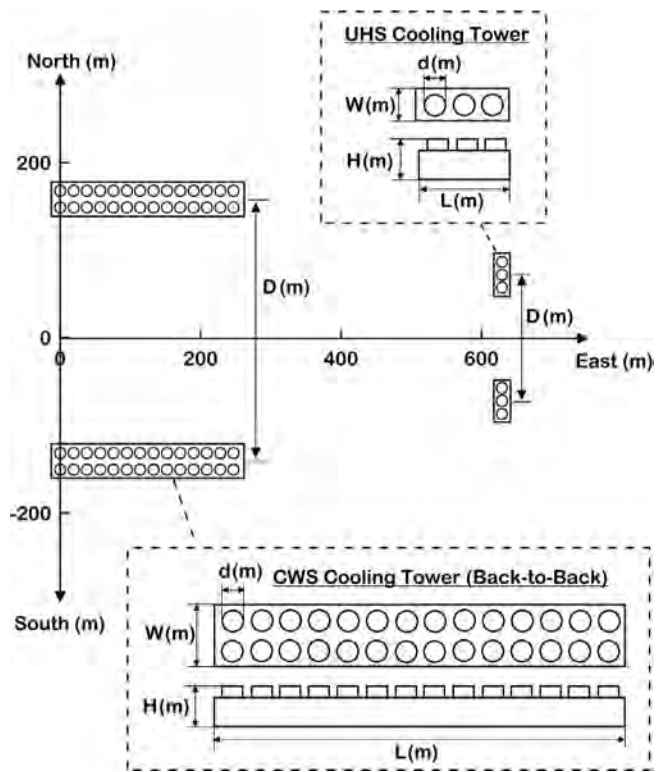

Fig. 2. Coordinate system for circulating water system (CWS) and ultimate heat sink (UHS) cooling towers.

during the operating modes of startup, shutdown, normal, and abnormal operations. The ambient design inlet wet-bulb temperatures of the cooling towers were obtained by adding 1.1 °C recirculation to 27.2 °C at 0% annual exceedance value for accident conditions and 26.2 °C at 5% annual exceedance values for normal plant operation, specified in the EPRI utility requirements document (EPRI, 2014). Unlike the CWS cooling towers, the maximum heat load of the UHS cooling towers of an APR1400 standard design plant varies depending on the modes of plant operation. The maximum heat load of the UHS

Table 1
The design parameters of CWS and UHS cooling towers of APR1400 standard design plant.

	CWS	UHS
Type	(Wet-type), mechanically induced draft back-to-back type concrete structure	Wet-type, mechanically induced draft counterflow linear type concrete structure
Safety function	Non-safety-related	Safety-related
Number of towers	2	4
Number of cells per tower	28	3
Inlet wet-bulb temperature (°C) including recirculation of 1.1 °C	27.2 for all conditions of normal plant operation	28.3 for accident condition 27.2 for normal plant operation
Inlet water temperature (°C)	40.7	37.6 (for normal operation) 43.7 (for 3.5 h after normal shutdown) 35.7 (for SIAS) 41.9 (for CSAS) 52.1 (for safe shutdown)
Outlet water temperature (°C)	32.4	32.1 for normal operation and shutdown 33.2 for accident and safe shutdown
Max heat load (MW)	2660.5 for Condenser 22.57 for TGBCCW HX Total: 2683.07 MW	37.7 (for normal operation) 80.2 (for 3.5 h after normal shutdown) 23.9 (for SIAS) 56.1 (for CSAS) 106.0 (for safe shutdown)

CWS: Circulating water system.
UHS: Ultimate heat sink.
SIAS: Safety injection actuation signal.
CSAS: Containment spray actuation signal.
TGBCCW HX: Turbine generator building component cooling water heat exchanger.

cooling tower was determined based on the heat load of 3.5 h after normal shutdown, which is about 30 times smaller than that of the circulating water cooling towers. Fig. 2 shows the coordinate system for the UHS and CWS cooling towers. Two CWS cooling towers with back-to-back arrangement are located in parallel along the east–west direction. The UHS cooling towers are arranged in series along the north-–south direction. The dashed rectangular lines show the enlarged top-view and front-view of CWS and UHS cooling towers.

The orientation of the linear mechanical draft cooling towers (LMDCTs) should be considered in the design of cooling towers because it has an effect on plume recirculation and interference depending on the prevailing wind direction. In general, to minimize recirculation and interference between cooling towers, the orientation of the cooling tower should be designed to be parallel to the prevailing wind direction. In this study, however, the orientation of cooling towers was applied with reference to the site plot plan of APR1400 standard design plant without considering prevailing wind direction.

2.2. SACTI2 model

The cooling tower plume prediction code, which is better known as SACTI, was developed by Policastro et al. (1984) and revised with the support of EPRI to improve the user friendliness of the code (Dunn et al., 1987). Compared to previous analytical models such as the cloud model by Orville et al. (1980) and the KUMULUS model by Moore (1977), the SACTI model provided improved plume behavior at high wind speeds. The main improvements of the SACTI model were as follows: improvement in how to select representative categories that hourly data are assigned to, calculation of ground sector shadowing for each hour, estimation of the solar insolation on a round, level horizontal surface, and estimation of the fractional sunlight beam energy loss, and rate of direct component of solar insolation absorbed by the plume (Carhart et al., 1992). To demonstrate the superiority of the SACTI model, Carhart et al. (1992) numerically investigated the difference in average annual horizontal surface energy loss assuming a single natural draft cooling tower (NDCT) with direct overhead sunlight all through the day, three NDCTs with the same heat loads, two nine-cell linear mechanical draft cooling towers (LMDCTs), and meteorological data for different sites. In terms of the theoretical superiority and better predictive performance, the SACTI model was calibrated and validated using an extensive US and European database on cooling tower plumes and drift by Policastro et al. (1994). Over the past two decades, however, some further issues have been raised by users and developers of the code. The original SACTI code was comprehensively upgraded by a technical advisory group (TAG) from the EPRI advanced nuclear technology (ANT) program, including the original SACTI model developers; the newly enhanced model with the fully-integrated structure is referred to as SACTI2 (EPRI, 2015). The major changes featured in SACTI2 are as follows: 1) restructuring of the code by converting from F77 to ANSI F90 protocol, 2) using a single user input file for the analysis, 3) removing known runtime bugs, 4) availability of an unlimited number of exit ports for mechanical draft cooling towers, 5) considering wind direction from all sectors of a 16-point compass rose instead of the equivalent wind directions, 6) assessing fogging and icing impacts during the day only, the night only, or both, and 7) generating outputs in either Cartesian or polar coordinates. The SACTI2 model is used for predicting annual and seasonal plume length/height/radius frequency, plume shadowing hours, solar energy loss on a horizontal
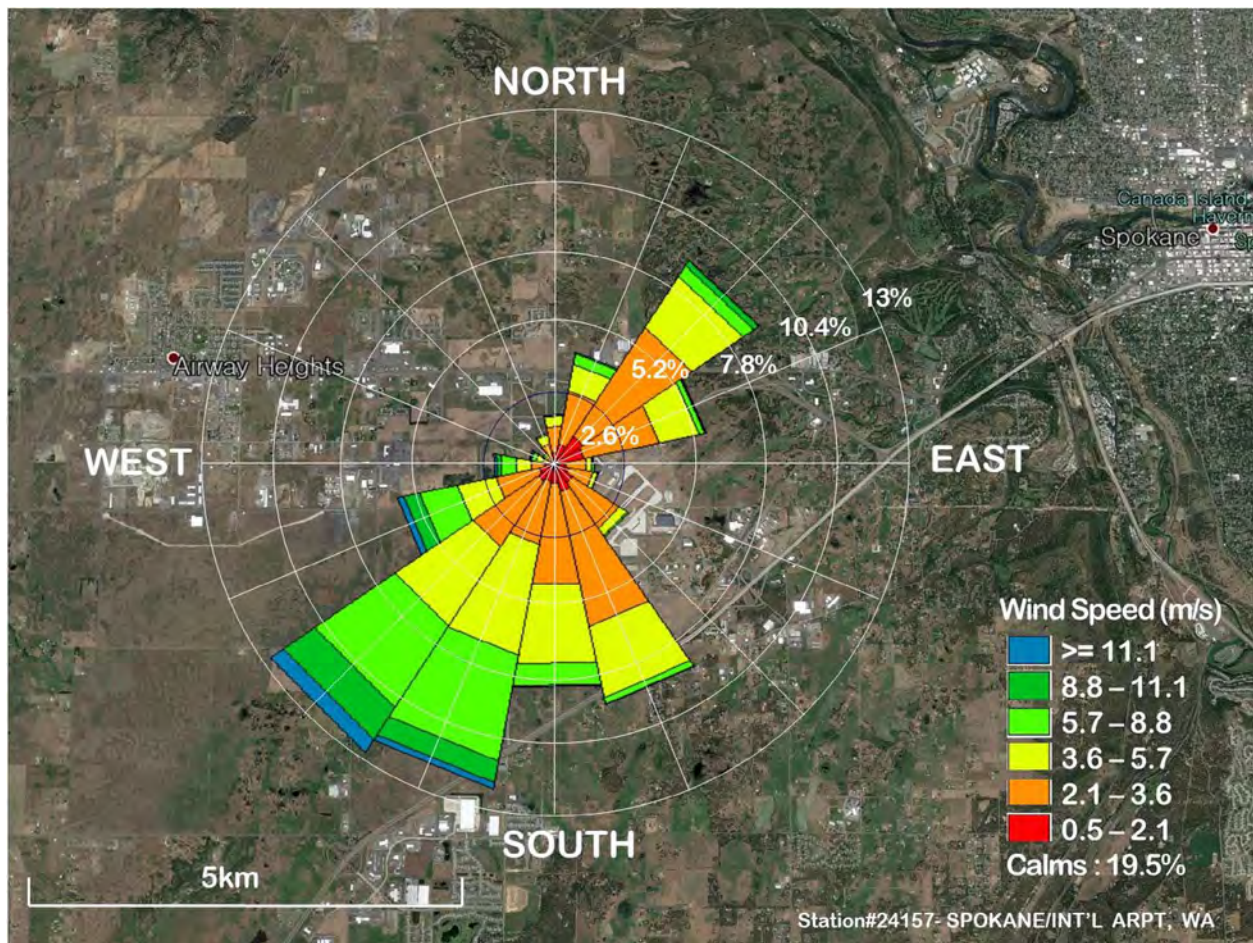

Fig. 3. Average wind rose for Spokane International Airport for 2013.

surface, fractional solar energy deposition loss, fractional beam energy deposition loss, plume salt deposition flux, plume water deposition flux, and plume fogging and icing. The main assumption of the core model used in the SACTI2 code includes that the impact assessment is conducted only at ground level, the topography of the site is flat, the assessment is applied to an area near cooling towers, and the exit ports of the cooling towers have the same height. In the SACTI2 model, the calculation is performed by following three main modules: 1) the preprocessor module for reading input data and generating representative cases for each plume category, 2) the plume module for determining plume and drift predictions for representative cases within each category, 3) the tables module for generating tables of predicted results. To execute the preprocessor module, at least one year of hourly surface meteorological data and concurrent twice-daily mixing heights are required. The user manual for SACTI2 provides information on how to get surface meteorological data such as a raw integrated surface database (ISD) file from the website (Smith et al., 2011) of the National Climate Data Center (NCDC) which was merged with the National Geophysical Data Center (NGDC) and the National Oceanic Data Center (NODC) into the National Centers for Environmental Information (NCEI) in 2015, and how to generate a modified ISD surface file for input to SACTI2 using a customized version of AERMET (EPA, 2004) which is a meteorological preprocessor for AERMOD (American Meteorological Society / Environmental Protection Agency regulatory model). Fig. 3 shows a one-year average wind rose with 4 km radius for the Spokane International Airport region. The Spokane International Airport is located on the plateau area at an elevation of 724.2 m and 9.7 km further away in west-southwest direction from the urban area of Spokane. In Fig. 3, the wind rose shows the frequency and speed of wind blowing from each direction. The wind rose is distributed in a northeast–southwest direction from the tower. The average wind speed and frequency of calm wind were 3.3 m/s and 19.5%, respectively. The dominant direction of the wind rose can be effectively used for analyzing contour values of the environmental assessment indexes. Table 2 shows the monthly based local meteorological data of Spokane International Airport in 2013. The climate of the Spokane International Airport has the characteristics of moist coastal weather in winter, and a mild, arid weather during the summer months.

2.3. Test conditions

In the environmental assessment for licensing, the site-specific land use and land cover should be considered for the potential impact of cooling towers. The cooling tower plume impacts focus on the growing season, not the entire year. The impacted areas are estimated based on modeled contours overlaid with a land use/land cover map using a geographic information system (GIS) technique along with the sensitivity of a receiving area to the impacting factors such as salt deposition and plume shadowing. However, since the site for the APR1400 standard plant has not been determined yet, the same meteorological data of Spokane International Airport as used in the SACTI2 user's manual were used as hypothetical meteorological data. This study aimed to quantify the effect of cooling tower design changes on the near-field

environment for only one year's meteorological data. The potential impact across test scenarios was compared in terms of the normalized dispersion ratio for each environmental assessment index without considering site-specific land use/land cover and growing season.

Table 3 shows the design parameters for test scenarios used. Ten test scenarios were applied to investigate how changing the design parameters of cooling towers affects the near-field environment. Test-1 was used as a reference assessment condition. Section 3.2 shows the environmental impact of cooling towers for Test-1 investigated in terms of the environmental assessment indexes. In Section 3.1, the analysis results for other test scenarios from Test-2 to Test-10 are quantitatively compared to that of Test-1.

In general, the location and arrangement of the UHS cooling towers have been negligible for the assessment using the SACTI model. However, the combined maximum heat loads adding CWS to UHS should be considered to conduct more conservative assessments for real environmental licensing. In Table 3, Test-1 is a scenario condition assuming that the CWS cooling towers alone operate and the UHS cooling towers are negligible. During normal plant operation, the heat load of the UHS cooling towers is orders of magnitude less than that of the CWS cooling towers. In Test-1, two CWS cooling towers with the separation distance of 299 m are located in parallel with a back-to-back arrangement which is effectively adapted to the plant site where the available area for the cooling towers is relatively small. The cooling tower with the back-to-back arrangement has 14 ports in each row as shown in the lower dashed rectangular box of Fig. 2. The height of each port is 16.9 m and the port diameter is 13.87 m. The width and length of the cooling tower housing are 38 m and 266 m, respectively. To remove a total heat load of 2683 MW, a total air flow rate of 27,681 kg/s is generated from 56 ports of two parallel cooling towers with the back-to-back arrangement.

Based on the condition of Test-1 as a reference scenario, other test scenarios including Test-2 to Test-10 were developed in two categories. The first group including Test-2 to Test-5 is related to changing arrangement and separation distance of cooling towers, and adding UHS cooling towers. Based on the Test-1, the arrangement of the CWS cooling towers in Test-2, the addition of UHS cooling towers in Test-3, and the separation distance between cooling towers in Test-4 and Test-5 were changed. The second group consisting of Test-6 to Test-10 is associated with changing the thermal design parameters of the cooling towers. The arrangement and the separation distance between cooling towers of the second group are the same as those of Test-1. However, the port diameter in Test-6, the port height in Test-7, a total port number that is related to changing the length of the tower housing in Test-8, a total heat load in Test-9, and a total air flow rate in Test-10 were changed to investigate the effect of changing thermal design condition of cooling towers on the environment.

In Test-2, each CWS cooling tower is designed in a longer inline arrangement with 28 ports in a row instead of a back-to-back arrangement with 14 ports in each row assuming a large available site area. Changing the general arrangement of the cooling tower involves the change of the length and width of the cooling tower housing. Compared with the layout of the cooling towers of Test-1, the width of

Table 2
Monthly-based local climatological data of Spokane International Airport (Station WBAN #24157) for 2013.

Meteorological Parameter	Jan.	Feb.	Mar.	Apr.	May	June	July	Aug.	Sep.	Oct.	Nov.	Dec.	Year
Average Dry Bulb Temp. (°C)	−4.1	1.0	0.0	7.8	13.8	16.5	23.3	22.3	17.2	7.6	1.6	−3.5	8.6
Highest Max. Temp. (°C)	6.1	10.0	20.0	22.8	30.0	32.8	37.2	33.3	33.3	19.4	11.1	6.7	21.9
Lowest Min Temp. (°C)	−15.6	−6.1	−5.6	−6.0	−1.0	6.7	10.6	11.1	5.6	−3.8	−9.3	−18.8	−2.7
Mean Wet Bulb Temp. (°C)	−4.3	−0.3	2.2	3.9	8.6	11.5	13.5	14.3	12.1	4.3	0.0	−4.4	5.1
Relative Humidity (%)	89	82	67	57	53	57	33	45	61	67	80	79	64
Wind Speed (m/s)	2.2	3.0	3.9	5.1	3.2	3.4	3.1	2.8	3.8	2.5	3.3	2.6	3.3
Prevailing Direction of Wind (Tens of Degrees)	21	21	20	22	20	20	22	23	6	5	4	17	22
Precipitation (cm)	4.14	1.88	2.08	2.39	2.03	4.72	Trace	1.73	3.96	0.23	3.96	1.73	28.85

Table 3
Design parameters for test scenarios.

Scenario Name	Modeled tower	Arrangement	TN	PN	D(m)	H(m)	d(m)	W(m)	L(m)	Total heat load (MW)	Total air flow rate (kg/s)
Test-1	CWS	BTB	2	56	299	16.90	13.87	38	266	2683	27,680.80
Test-2	CWS	Inline	2	56	299	16.90	13.87	19	532	2683	27,680.80
Test-3	CWS/UHS	BTB/Inline	2/2	56/6	299/100	16.90	13.87	38/19	266/42	2763	30,646.60
Test-4	CWS	BTB	2	56	349	16.90	13.87	38	266	2683	27,680.80
Test-5	CWS	BTB	2	56	199	16.90	13.87	38	266	2683	27,680.80
Test-6	CWS	BTB	2	56	299	16.90	9.80	38	266	2683	27,680.80
Test-7	CWS	BTB	2	56	299	19.80	13.87	38	266	2683	27,680.80
Test-8	CWS	BTB	2	40	299	16.90	13.87	38	190	2683	27,680.00
Test-9	CWS	BTB	2	56	299	16.90	13.87	38	266	3080	27,680.80
Test-10	CWS	BTB	2	56	299	16.90	13.87	38	266	2683	33,600.00

CWS: Circulating water system.
UHS: Ultimate heat sink.
BTB: Back to back.
TN: Number of towers.
PN: Number of ports.
D: Distance between two parallel cooling towers.
H: Height of a tower.
d: Port diameter.
W: Width of the tower housing.
L: Length of the tower housing.

the cooling tower housing in Test-2 is reduced to 50%, but the length of the cooling tower housing is designed to be up to 50% longer. Test-3 has the most conservative condition for the environmental assessment in terms of assuming that both the CWS and UHS cooling towers operate. The location of the cooling towers for Test-3 is shown in Fig. 2. This condition should be used in the environmental assessment for licensing. In the case of Test-4, the perpendicular separation distance between CWS cooling towers in two back-to-back arrangements is increased by 33.4% in comparison with Test-1. In Test-5, the separation distance between two CWS cooling towers is reduced by 33.4%.

In terms of thermal design of cooling towers, the port diameter, a total number of ports, the port height will be determined depending on which performance fan and what type of fill are applied to the cooling tower design. Thus, changing thermal design of fans and fills inside the cooling tower has effect on the layout of the cooling towers in Test-6 to Test-8. In Test-6, the port exit diameter decreases to 29.3%. Because the port diameter in Test-6 is smaller than that of Test-1, the size of a fan in each port in Test-6 would be smaller than that of Test-1. However, a total heat load of cooling towers in Test-6 is the same as that of Test-1. The air flowrate required for each port in Test-6 should be the same as that of Test-1. Accordingly, the cooling tower fan inside each port in Test-6 should have better thermal performance; for example, it should be operated at much higher speed. Otherwise, in Test-6, cooling tower fills with higher performance should be used to increase the cooling capacity inside the cooling towers. In Test-7, the exit port height increases to 17.2%, compared to that of Test-1. As the port height in Test-7 is higher than that of Test-1, more fills can be inserted inside the cooling towers. In that regard, the same heat load as Test-1 can be removed using fans and fills with lower performance in Test-7. The number of ports in Test-8 is 16 fewer than that of Test-1 even though the diameter of each port in Test-1 and Test-8 is the same; Test-8 has 40 ports, but Test-1 has 56. The total heat load and total air flow rate are the same for Test-1 and Test-8. Therefore, more heat load at each port in Test-8 should be removed in comparison with Test-1. This means more air flow rate should be provided by a fan in each port of Test-8. Otherwise, high-performance fills should be used to increase the cooling capacity at each port in Test-8. In Test-9, the total heat load of the CWS cooling towers is increased to 14.8% more than that of Test-1. In Test-10, the port air flow rate increases to 21.4% in comparison with Test-1.

3. Results and discussions

3.1. Impact of visible plume for Test-1

Plume produced from cooling towers can be visible due to the condensation of the water vapor with ambient air. The levels of the moisture of plumes depend on the meteorological condition for ambient air. Such plumes behave like clouds, decreasing the amount of solar energy on a horizontal surface, and therefore have adverse effects on the surrounding residential area and vegetation. For example, they can be sometimes misidentified as fire or pollutants, look aesthetically bad, obscure the view on a surface in the form of fogging, and decrease crop yield by blocking and scattering the sunlight across farmland. Accordingly, predicting seasonal and annual average behavior of the visible plumes near cooling towers is necessary for environmental assessment. The SACTI-2 model is able to predict the impact of visible plumes on the environment with several environmental assessment indexes: plume length frequency (PLF), plume shadowing hour (PSH), plume fogging hour (PFH), plume icing hour (PIH), plume salt deposition flux (PSDF), plume water deposition flux (PWDF), fractional solar energy deposition loss (FSDL), fractional beam deposition loss (FBDL), and total solar energy loss (TSL).

3.1.1. Plume length and shadowing

A typical contour plot of annual average plume length frequency (PLF) for Test-1 is shown in Fig. 4. The isopleths represent the PLF of occurrence in percentage, which is a ratio of the time when visible plumes are observed to the total recording time per year. The maximum value of PLF is 14.12%, which represents the ratio of visible plume observation time of 1204 h to the total recording time of 8527 h per year. In Fig. 4, PLF larger than 1% is observed to mainly disperse within a 4 km radius from the starting point of the coordinate system according to the northeast–southwest direction. Fig. 5 shows a typical contour plot of annual average plume shadowing hours (PSH) for Test-1. The contour lines show predicted hours with shadows on the ground near the power plant region due to the presence of visible plumes from cooling towers. The PSH is observed larger than 10 h within a 4 km radius from the starting point of the coordinate system. The maximum PSH is 1899 h, which accounts for 22.3% of the total record time of 8527 h. The higher levels of PSH are observed within a 0.2 km radius.

3.1.2. Fogging and icing

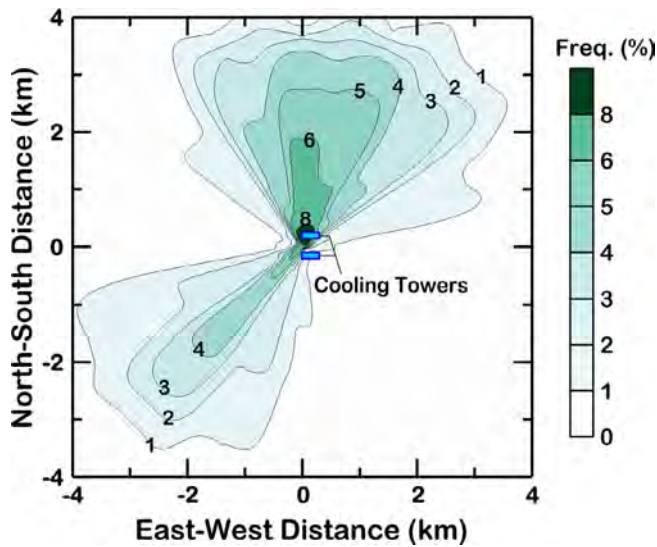Visible plume from cooling towers rises or falls to ground level

Fig. 4. Typical contour plot of annual average plume length frequency (PLF) for Test-1 condition.
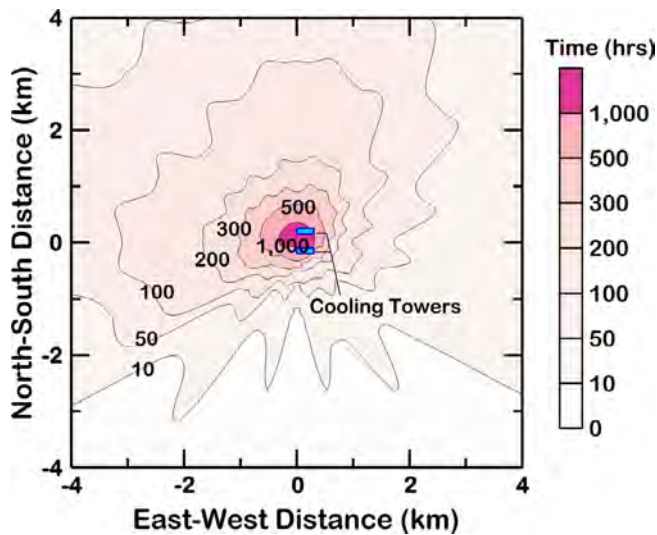

Fig. 5. Typical contour plot of annual average plume shadowing hours (PSH) for Test-1 condition.

depending on meteorological conditions such as ambient temperature, ambient pressure, and wind direction. When a visible plume touches the ground in the meteorological condition of positive ambient temperature, it generates plume-induced fogging on the ground. Fig. 6 shows the prediction of the plume-induced fogging on the ground for Test-1. The plume fogging hours (PFH) are distributed in a northeast–southwest direction aligning with prevailing wind directions. The dispersion pattern in the northeast–southwest direction looks similar to that of PLF. The maximum value of fogging hours is predicted to be 30.23, and the isopleth of one hour lies within a 1 km radius distance normally falling within plant boundaries. The plume-induced icing may occur when the visible plumes intersect the ground at below-freezing temperature. It is strongly influenced by ambient temperature and wind direction during the winter season. Fig. 7 shows the predicted hours with plume-induced icing on the ground for Test-1. It is observed that the area of plume-induced icing extends to the level of 0.2 h in a 1 km radius toward the southwest direction. The dispersion pattern of plume icing hours (PIH) is not like that of plume-induced fogging hours because it is influenced by only the winter season meteorological conditions.

3.1.3. Salt and water depositions

While cooling towers operate, liquid water droplets (also known as drift) are discharged from the cooling towers. Mineral salts and water are deposited as the drift droplets falling from cooling tower plumes intersect the ground surface. Any type of deposition on the ground can reduce the cooling efficiency of the cooling towers and may have adverse effects on the environment. Plants are generally not damaged by salt deposition rates of 100–200 kg/km^2 per month. Salt deposition rates greater than 1000 kg/km^2 per month during the growing season have the potential to cause leaf damage in some vegetation species (U.S. NRC, 2007). The SACTI2 model can calculate the water and salt deposition flux in kg/km^2 per month from the drift escaping from the cooling tower. Fig. 8 shows a predicted annual plume salt deposition flux (PSDF). The maximum salt deposition flux is 9555 kg/km^2 per month.

A predicted annual plume water deposition flux (PWDF) is shown in Fig. 9. The maximum value of the water deposition flux is 1,820,000 kg/km^2 per month. The same dispersion pattern within a 1 km radius from the center of the coordinate system is observed in the contour plots of PSDF and PWDF. The maximum salt and water depositions are distributed in a northeast–southwest direction along the prevailing wind directions. However, the maximum values differ by two orders of magnitude. The salt and water deposition fluxes decrease beyond a 1 km radius further away from the center of the coordinate system, less than 50 kg/km^2 per month and 7000 kg/km^2 per month, respectively.

3.1.4. Solar energy losses

Plume shadowing has a great impact on annual average solar insolation. Visible sunlight consists of a direct beam and a diffuse component on a horizontal surface. The direct beam is easily removed by plume shadowing, whereas the diffuse component is not affected (Carhart et al., 1992). Fig. 10 shows the contour plot of the fractional solar energy deposition loss (FSDL) in percentage for Test-1. The FSDL is distributed in the predominant wind direction and characterized with the general northward shift observed in the Northern Hemisphere. FSDL larger than 1% is observed to mainly disperse within a 4 km radius from the starting point of the coordinate system. Fig. 11 shows the predicted annual fractional beam energy deposition loss (FBDL) incident on the ground due to plume shadowing in percentage. The direct beam energy loss is distributed in the same direction as FSDL. FBDL larger than 1% is observed to mainly disperse according to the predominant wind direction with the general northward shift observed in the Northern Hemisphere within a 4 km radius from the starting point of the
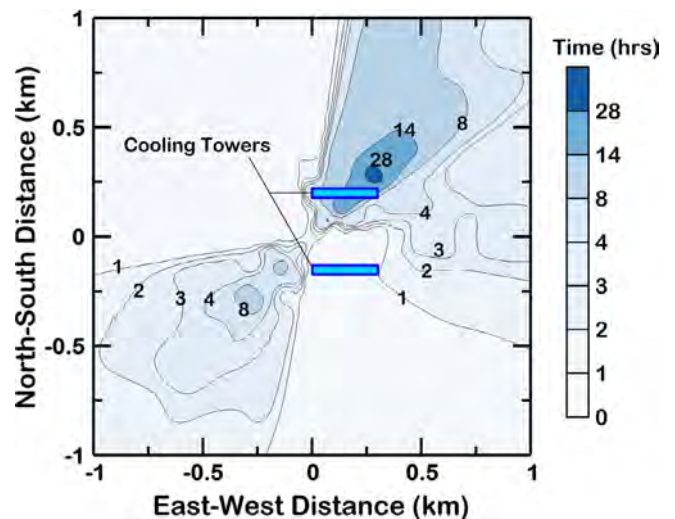

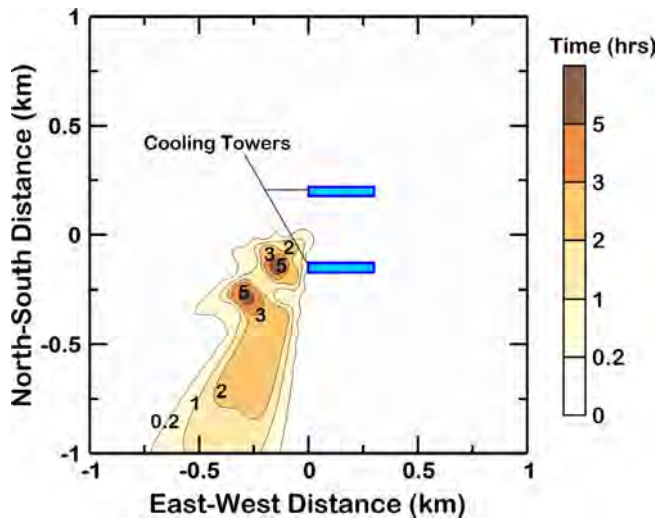**Fig. 6.** Typical contour plot of annual average plume fogging hours (PFH) for Test-1 condition.

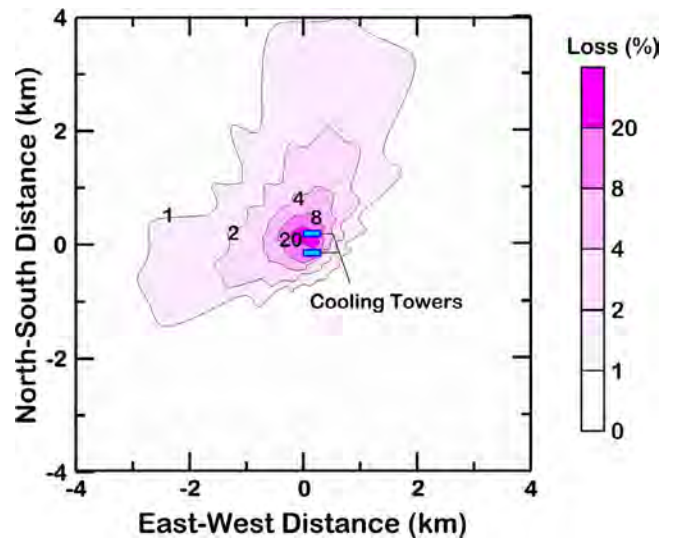**Fig. 7.** Typical contour plot of annual average plume icing hours (PIH) for Test-1 condition.
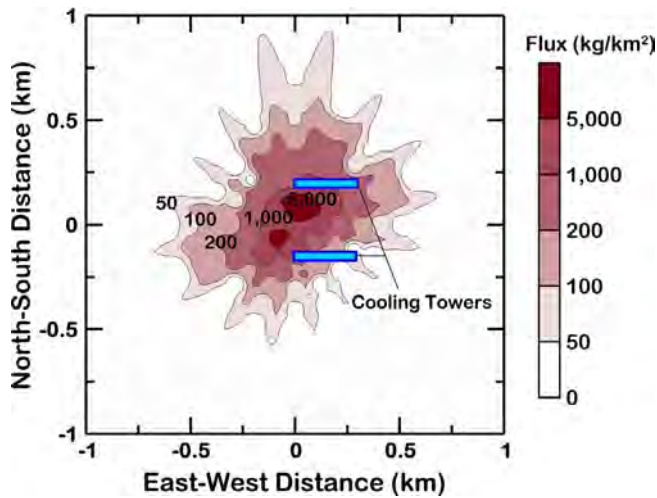

Fig. 8. Typical contour plot of annual average plume salt deposition flux (PSDF) for Test-1 condition.

Fig. 9. Typical contour plot of annual average plume water deposition flux (PWDF) for Test-1 condition.
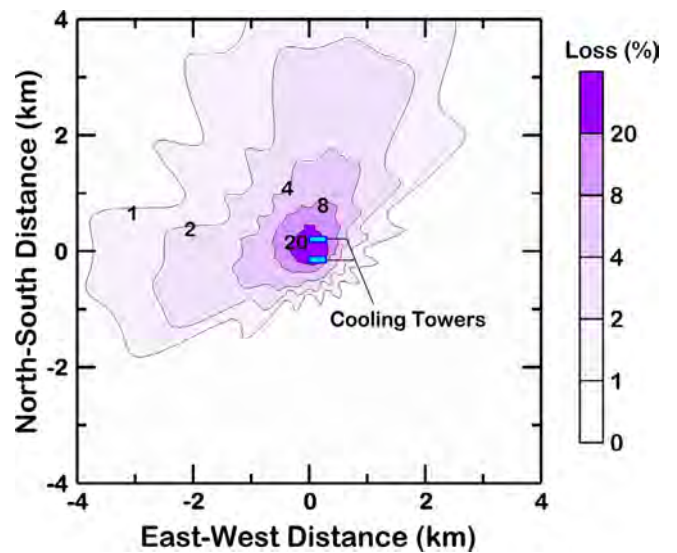

Fig. 10. Typical contour plot of annual average fractional solar energy deposition loss (FSDL) for Test-1 condition.
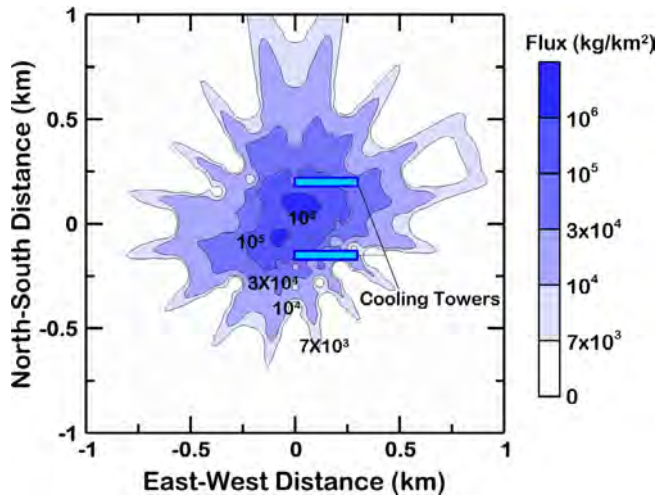

Fig. 11. Typical contour plot of annual average fractional beam energy deposition loss (FBDL) for Test-1 condition.

coordinate system. Fig. 12 illustrates the annual total solar energy loss (TSL) in MJ/m^2 on a horizontal surface due to plume shadowing. The maximum value of the TSL is 1293 MJ/m^2. The TSL is distributed mainly along a northeast–southwest direction, consistent with plume shadowing hours being stronger to the northeast of the cooling towers. The TSL larger than 20 MJ/m^2 is observed to mainly disperse within a 4 km radius from the starting point of the coordinate system.

3.2. Effect of cooling tower design change

As described in Section 2.2, the environmental assessment indexes are calculated for different subsectors in the 16 wind rose directions from the starting point in the coordinate system. The grid for the two dimensional contour plots of the environmental assessment indexes is composed of the subsectors. Each grid has a value corresponding to an environmental assessment index. The index-value dispersion area (A_D) is newly defined to quantify the effect of the cooling tower on the environment, which is a summation of areas of subsectors whose index value is the same or larger than an interested index value in the grid. It is calculated as follows:
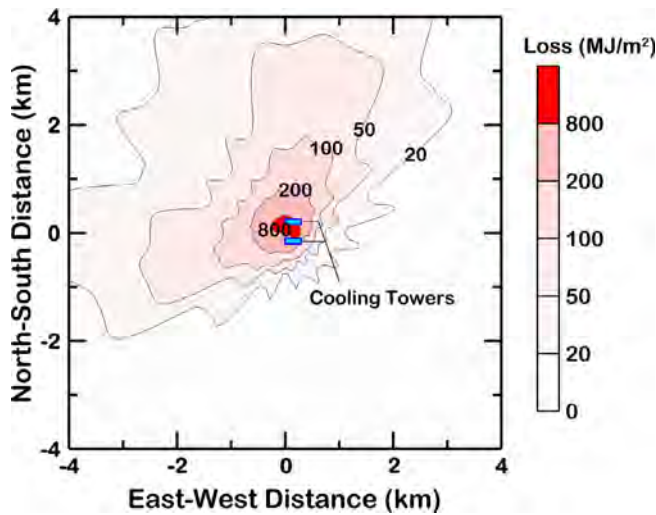
Fig. 12. Typical contour plot of annual average total solar energy loss (TSL) for Test-1 condition.

$$A_D = \sum_{j=1}^{n} \sum_{i=1}^{m} N_{ij} \times S_j$$

where n denotes the number of the radial locations from the starting point of the coordinate system for the index value measurement and m is the number of the wind rose direction used in the model. The location of the subsectors can be expressed using indexes i and j. The parameter S_j is the area of subsector in the jth ring and N_{ij} is assigned 0 or 1 for the ith subsector in the jth ring depending on whether an index value is the same or larger than an interested index value. The maximum value of n and m used was 100 and 16, respectively. Thus, the maximum number of the subsectors used in the model was 1600. The dispersion ratio (δ) is to investigate the effect of cooling towers on the environment for each environmental assessment index. Even though the dispersion ratio is not necessarily an indicator for environmental impact, it can be useful to design the cooling towers considering the environmental impact. It is calculated by normalizing the index-value dispersion area (A_D) by the region-of-interest area (A_O) as follows:

$$\delta = A_D/A_O$$

The normalized dispersion ratio ($\delta_{Test}/\delta_{Test-1}$) is the ratio of the normalized index-value dispersion area of each test scenario to that of Test-1. It is used to quantitatively investigate the effect of the cooling

tower design change on the environment. The quantitative comparison for design changes of cooling towers is shown in Figs. 13–21. As mentioned in Section 2.3, the test scenario conditions from Test-2 to Test-10 is categorized into two parts based on the reference test scenario, Test-1. The first group relating to the change of cooling tower arrangement is shown in Figs. 13(a)–21(a), whereas the second group associated with thermal design change is shown in Figs. 13(b)–21(b).

3.2.1. Plume length and shadowing

The normalized dispersion ratio for plume length frequency (PLF) values at different test conditions is shown in Fig. 13(a) and (b). The normalized dispersion ratio changes significantly when the thermal performance is changed rather than when changing the cooling tower general arrangement. As shown in the contour lines in Fig. 4, PLF is high in the area close to the cooling tower, but PLF is lower the farther it gets from the cooling tower. For the same PLF value, if the area of each test case is larger than the area of Test-1, the normalized dispersion ratio is larger than 1. In Test-1, the PLF of 6.5 is distributed in about a 2 km radius area from the center of the cooling tower. In Fig. 13(b), the normalized dispersion ratio of Test-9 has the maximum PLF value of 6.5, which means that the area of PLF ≥ 6.5 in Test-9 is roughly 3.5 times larger than that of Test-1. Variation of the normalized dispersion ratio for PLF is most evident in Test-8 and Test-9. Compared to Test-1, the number of ports in Test-8 decreases, but the total heat load is the same. This means that the heat load at each port increases and the amount of plume generated at each port also increases. Because of this, the normalized dispersion ratio of Test-8 reaches a maximum value of 2.1. However, when PLF is less than 6.5%, the normalized dispersion ratio becomes smaller. The total heat load of Test-9 is higher than that of Test-1; the number of exit ports of Test-9 is larger than that of Test-8. Therefore, each port of Test-9 generates the same amount of plume as Test-8, but the total amount of plume generated in the entire exit port would be the highest among all test cases. For this reason, the normalized dispersion ratio of Test-9 increases to 3.5. However, when PLF becomes smaller than 6.5%, the normalized dispersion ratio decreases. Since the normalized dispersion ratio for PLF is high when the amount of plume generated at each exit port is high, the normalized dispersion ratio for PLF is highly affected by the heat load variation.

Fig. 14(a) and (b) illustrates the normalized dispersion ratio for plume shadowing hours (PSH) values at different test conditions. The normalized dispersion ratio changes for PSH were notable in Test-2 and Test-3, as shown in Fig. 14(a). In the case of Test-2 designed as an inline cooling tower, the area where PSH is greater than or equal to 850 h is more than three times larger than that of Test-1. Compared to the back-
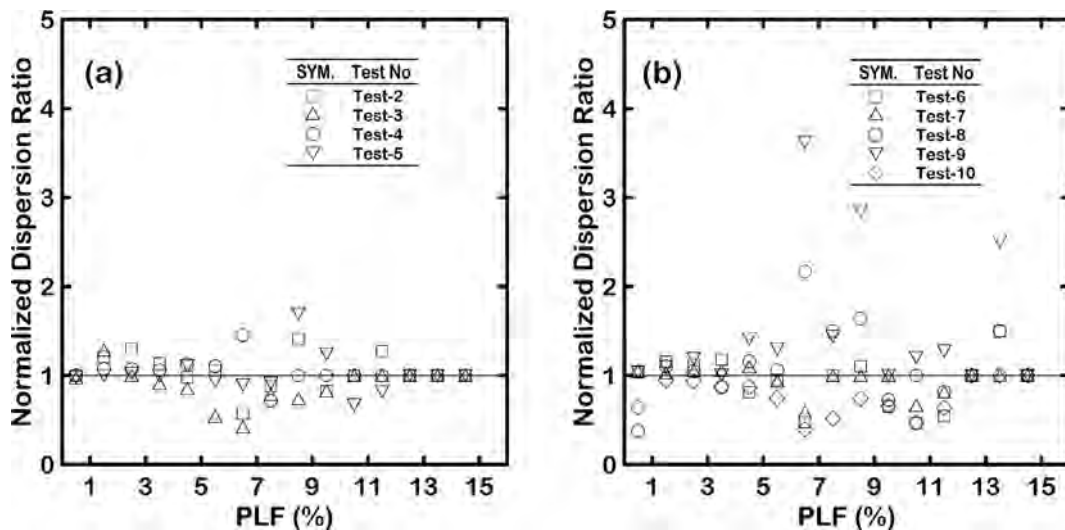

Fig. 13. Normalized dispersion ratio for plume length frequency (PLF) values at different test conditions.
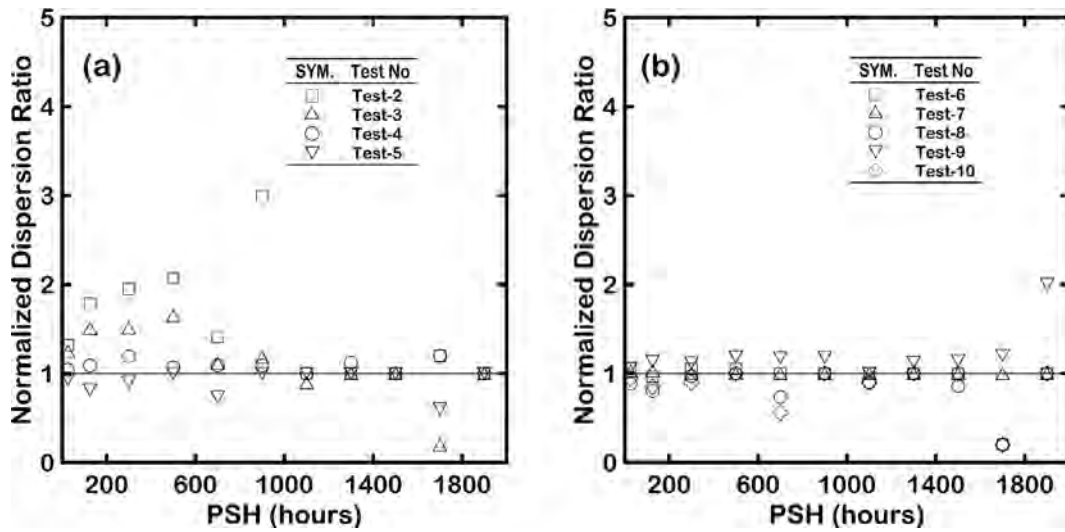
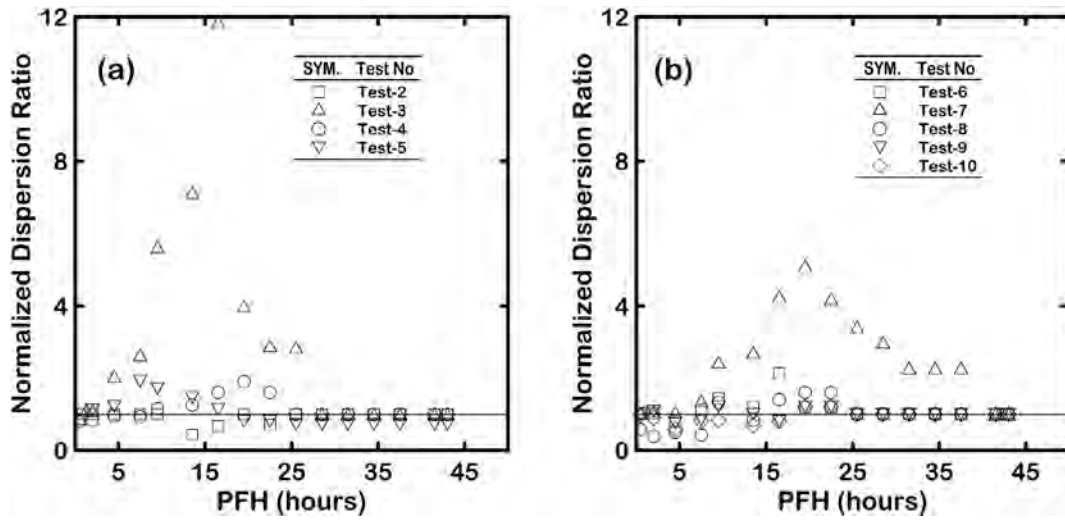**Fig. 14.** Normalized dispersion ratio for plume shadowing hours (PSH) values at different test conditions.

Fig. 15. Normalized dispersion ratio for plume fogging hours (PFH) values at different test conditions.
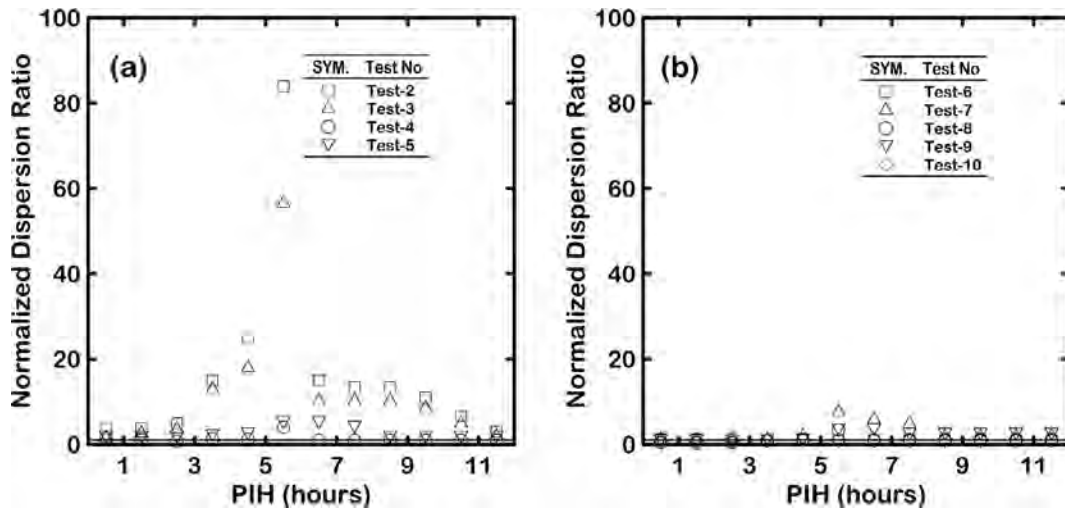

Fig. 16. Normalized dispersion ratio for plume icing hours (PIH) values at different test conditions.
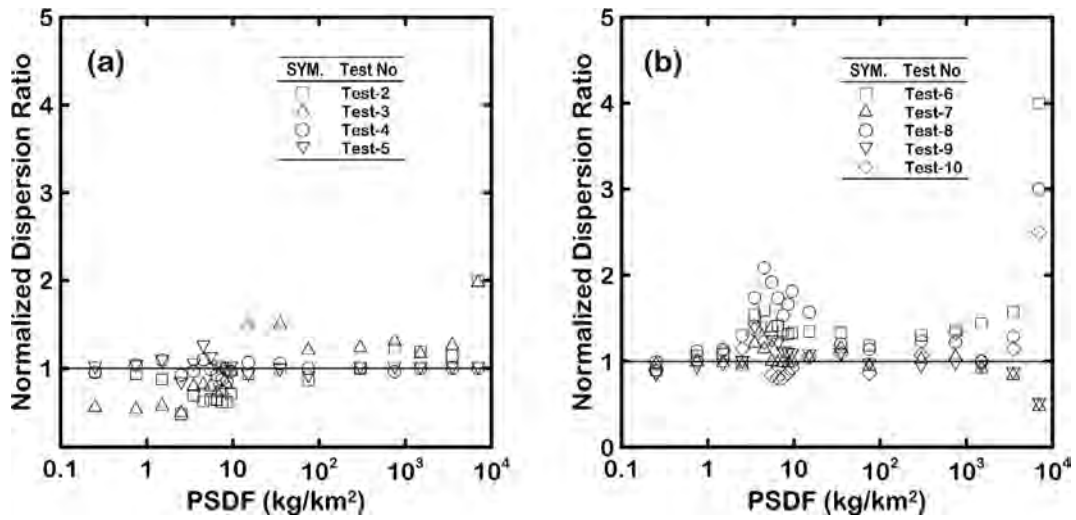
Fig. 17. Normalized dispersion ratio for plume salt deposition flux (PSDF) values at different test conditions.
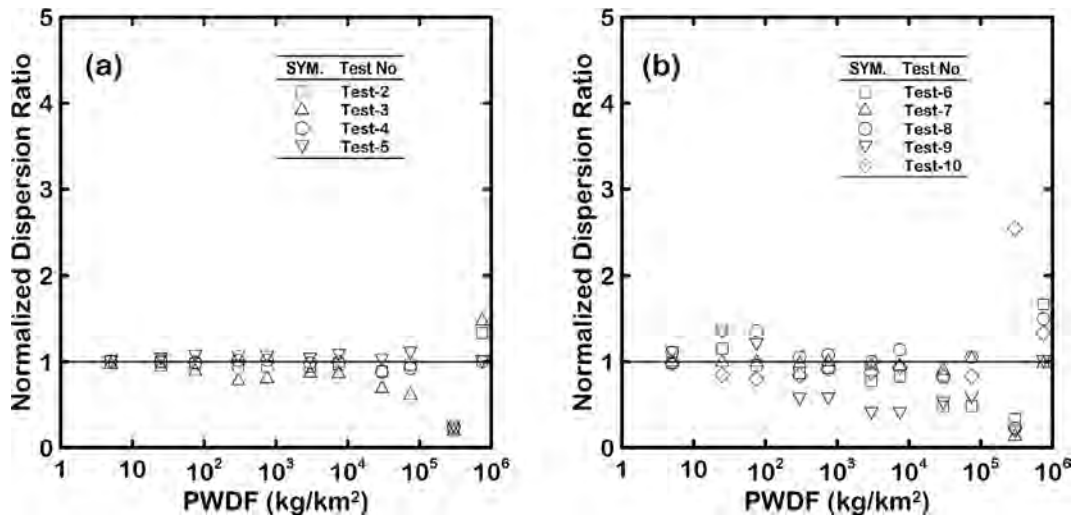

Fig. 18. Normalized dispersion ratio for plume water deposition flux (PWDF) values at different test conditions.
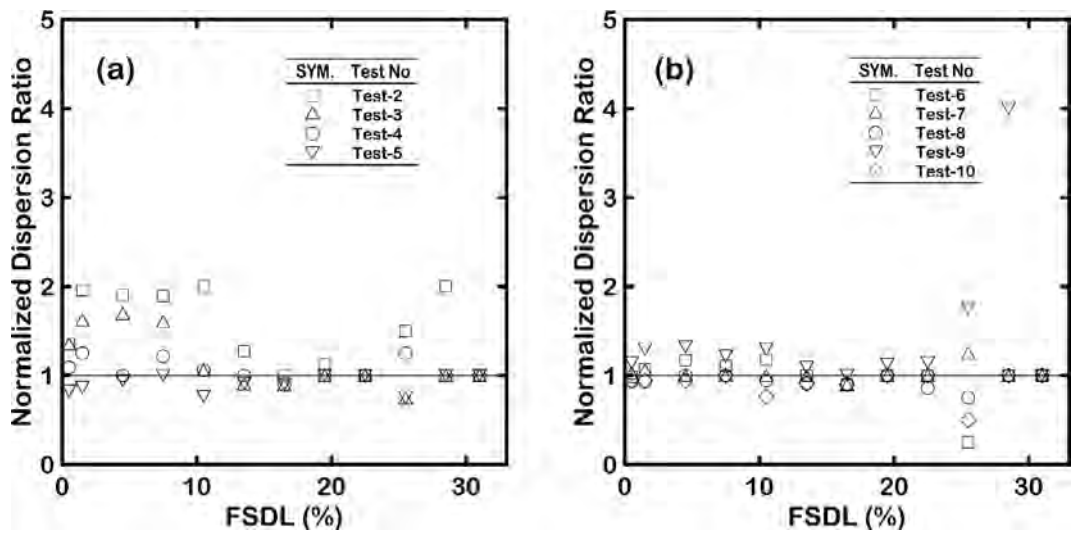

Fig. 19. Normalized dispersion ratio for fractional solar energy deposition loss (FSDL) values at different test conditions.
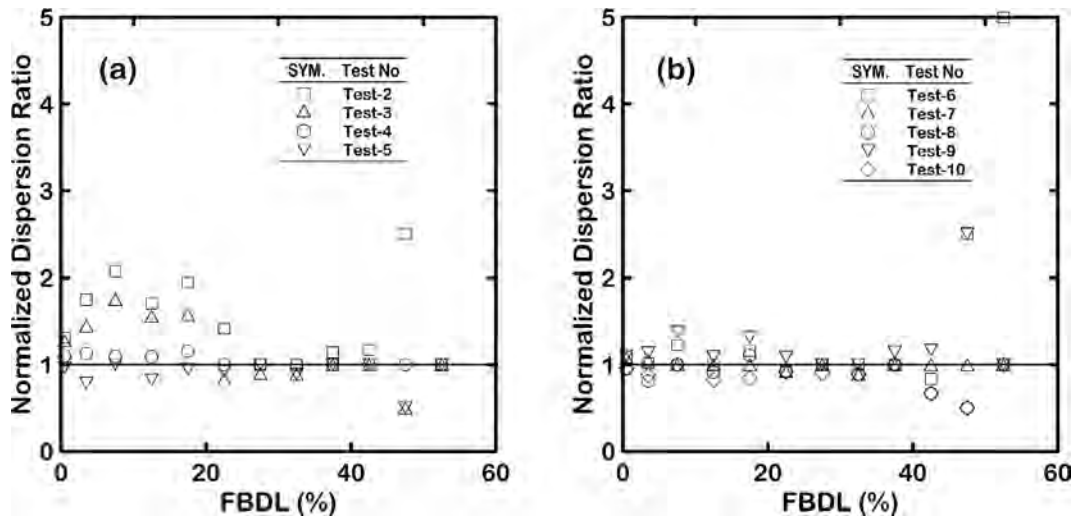
Fig. 20. Normalized dispersion ratio for fractional beam energy deposition loss (FBDL) values at different test conditions.
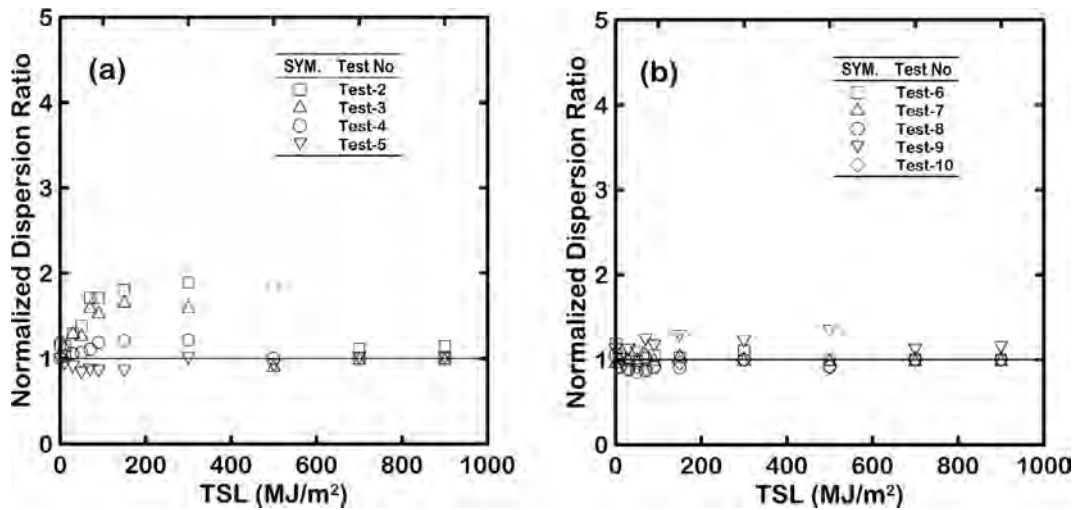

Fig. 21. Normalized dispersion ratio for total solar energy loss (TSL) values at different test conditions.

to-back arrangement, the plume yielded from the exit port of the cooling towers with the longer inline arrangement is more affected by the wind and is distributed over a wider area. Therefore, PSH increases further away from the cooling tower. In Test-3, UHS cooling towers are located about 500 meters east from the center of the CWS cooling tower, as shown in Fig. 2. As an additional plume generates from the UHS cooling towers, the plume in Test-3 is distributed over larger areas further away from the plant site depending on wind direction.

3.2.2. Fogging and icing

The normalized dispersion ratio for plume fogging hours (PFH) values at different test conditions is illustrated in Fig. 15(a) and (b). The region-of-influence of PFH is set to $1 \times 1 \, km^2$, as shown in Fig. 6. The maximum normalized dispersion ratio for PFH is 7, which is somewhat higher than for other environmental indexes. In Fig. 15(a), the normalized dispersion ratio for PFH is most prominent at the condition of Test-3. The dispersion area of plume-induced fogging in Test-3 increases because visible plume is distributed over a larger area due to the addition of UHS cooling towers. At the condition of PFH = 10–40 of Fig. 15(b), the normalized dispersion ratio for Test-7 with a higher exit port height increases, reaches the maximum value, and then decreases.

Fig. 16(a) and (b) shows the normalized dispersion ratio for plume icing hours (PIH) at different test conditions. The maximum normalized dispersion ratio for PIH is 84 at the condition of Test-2 with the longer

inline arrangement, which is a very large value by comparison with other environmental indexes. This is because plume produced from exit ports spreads to a wider area along the cooling towers in the longer inline arrangement. Moreover, in Test-3, the plumes spread to a wider area further away from the power plant. As more plumes due to the addition of UHS cooling towers reach the wider ground area, the normalized dispersion ratio for PIH increases. The normalized dispersion ratio for PIH is less affected by thermal design changes, as shown in Fig. 16(b).

3.2.3. Salt and water depositions

The normalized dispersion ratios for plume salt deposition flux (PSDF) and plume water deposition flux (PWDF) are shown in Figs. 17 and 18. The normalized dispersion ratio for the PSDF has a maximum value of 4 for Test-6 with decreased exit port diameter at the condition of PSDF = 10,000, as shown in Fig. 17(b). At the same condition, the normalized dispersion ratio for PSDF reaches a maximum value of 3 for Test-8 with decreased exit port numbers. When the exit port diameter becomes smaller or the exit port numbers decrease, more drift droplets yield from the cooling towers. Increased droplets falling from the cooling towers increase the value of PSDF near the cooling tower region.

At the condition of PWDF = 300,000 kg/km^2, the values of the normalized dispersion ratio for all the test scenario conditions except

Test-10 are smaller than 1. However, the value of the normalized dispersion ratio for Test-10 increases up to a maximum value of 2.5. This is because with increasing air flowrate per exit port, more water from drift droplets would be deposited near the cooling tower region. At the higher levels of deposition flux, the normalized dispersion ratios for PSDF and PWDF are more affected by thermal design changes of cooling towers.

3.2.4. Solar energy losses

The normalized dispersion ratios for fractional solar energy deposition loss (FSDL), fractional beam energy deposition loss (FBDL), and total solar energy loss (TSL) are illustrated in Figs. 19–21, respectively. Solar energy loss occurs because visible plumes due to the cooling towers block the solar heat reaching the surface. Therefore, FSDL, FBDL, and TSL should be analyzed in terms of plume shadowing hours (PSH) due to visible plumes generated from the cooling tower. The normalized dispersion ratio for PSH is more affected by changing cooling tower arrangement, especially for Test-2 and Test-3. Similar to the results for PSH in Fig. 14(a), the normalized dispersion ratios for FSDL, FBD, and TSL are predicted to be high at the condition of Test-2 and Test-3. If the plume generated from the cooling tower is distributed widely due to the change of cooling tower arrangement, FSDL, FBD, and TSL increase because the increased distribution area of PSH blocks more solar heat.

4. Summary

The impact of changing the design of CWS and UHS cooling towers for an APR1400 standard design plant on the near-field environment was investigated numerically using the SACTI2 model. Meteorological data near Spokane International Airport were used as hypothetical input data for the environmental assessment.

In Test-1, the distribution pattern of environmental assessment indexes excluding PIH is observed in a northeast and southwest direction according to prevailing wind directions. PIH is dispersed in a southwest direction only due to the effect of wind direction during the winter season. The environmental assessment indexes are distributed in the near-field regions from the cooling towers: within a 4 km radius for PLF and PSH, 1 km radius for PFH and PIH, 0.3 km radius for PSDF and PWDF, and 2 km radius for FSDL, FBDL, and TSL.

The index-value dispersion area (A_D) and dispersion ratio (δ) were defined and used to quantify the effect of cooling towers on the environment for each environmental assessment index. In addition, the normalized dispersion ratio by the environmental assessment index of Test-1 was used to investigate the impact of changing the general arrangement and design of cooling towers on the environment. The main conclusions for the impact of changing the general arrangement and design of cooling towers on the environment are as follows:

1. PLF is more affected by changing the thermal design such as in total heat load and the number of exit ports, whereas PSH is sensitive to the changing of the general arrangement of cooling towers such as in an inline arrangement and the addition of UHS cooling towers. The normalized dispersion ratio of solar energy losses including FSDL, FBDL, and TSL has the same effect as PSH.
2. PFH is affected by the addition of UHS and increased exit port height, whereas PIH is highly influenced by inline arrangement and the addition of UHS.
3. PSDF and PWDF are influenced by decreased port diameter, decreased port numbers, and increased air flow rate at the higher levels of PSDF and PWDF.

References

Carhart, R.A., Policastro, A.J., 1991. A second-generation model for cooling tower plume rise and dispersion - I. single sources. Atmos. Environ. Part A Gen. Top. 25 (8), 1559–1576. http://dx.doi.org/10.1016/0960-1686(91)90015-Y.

Carhart, R.A., Policastro, A.J., Dunn, W.E., 1992. An improved method for predicting seasonal and annual shadowing from cooling tower plumes. Atmos. Environ. Part A Gen. Top. 26 (15), 2845–2852. http://dx.doi.org/10.1016/0960-1686(92)90022-D.

Chahine, A., Matharan, P., Wendum, D., Musson-Genon, L., Bresson, R., Carissimo, B., 2015. Modelling atmospheric effects on performance and plume dispersal from natural draft wet cooling towers. J. Wind Eng. Ind. Aerodyn. 136, 151–164. http://dx.doi.org/10.1016/j.jweia.2014.11.007.

Davis, L.R., 1998. Fundamentals of Environmental Discharge Modeling. CRC Press, Boca Raton, FL.

Dunn, W., Coke, L., Policastro, A.J., 1987. User's Manual: Cooling Tower Plume Prediction Code (Revision 1), A Computerized Methodology for Predicting Seasonal/annual Impacts of Visible Plumes, Drift, Fogging, Icing, and Shadowing from Single and Multiple Sources. Research Project 906-1, Argonne National Laboratory, prepared for Electric Power Research Institute, Palo Alto, CA. https://www.nrc.gov/docs/ML1408/ML14087A352.pdf.

EPRI, 2012. Program on Technology Innovation: Tradeoffs between Once-through Cooling and Closed-Cycle Cooling for Nuclear Power Plants, EPRI TR-1025006. Electric Power Research Institute, Palo Alto, CA. https://www.epri.com/#/pages/product/000000000001025006/.

EPRI, 2014. Advanced Nuclear Technology: Advanced Light Water Reactor Utility Requirements Document (Revision 13), EPRI TR-3002003129. Electric Power Research Institute, Palo Alto, CA. https://www.epri.com/#/pages/product/3002003129/.

EPRI, 2015. User's Manual for the Seasonal/Annual Cooling Tower Impact Model Version 2 (SACTI2) A Computerized Methodology for Predicting Seasonal and Annual Impacts of Visible Plumes, Drift, Fogging, Icing and Shadowing from Single and Multiple Sources, EPRI TR-3002004259. Electric Power Research Institute, Palo Alto, CA. https://www.epri.com/#/pages/product/3002006350/.

Lucas, M., Martinez, P.J., Ruiz, J., Kaiser, A.S., Viedma, A., 2010. On the influence of psychrometric ambient conditions on cooling tower drift deposition. Int. J. Heat Mass Transf. 53 (4), 594–604. http://dx.doi.org/10.1016/j.ijheatmasstransfer.2009.10.037.

Meroney, R.N., 2008. Protocol for CFD prediction of cooling-tower drift in an urban environment. J. Wind Eng. Ind. Aerodyn. 96 (10), 1789–1804. http://dx.doi.org/10.1016/j.jweia.2008.02.029.

Michioka, T., Sato, A., Kanzaki, T., Sada, K., 2007. Wind tunnel experiment for predicting a visible plume region from a wet cooling tower. J. Wind Eng. Ind. Aerodyn. 95 (8), 741–754. http://dx.doi.org/10.1016/j.jweia.2007.01.005.

Milosavljevic, N., Heikkilä, P., 2001. A comprehensive approach to cooling tower design. Appl. Therm. Eng. 21 (9), 899–915. http://dx.doi.org/10.1016/S1359-4311(00)00078-8.

Moore, R.D., 1977. The KUMULUS Model for Plume and Drift Deposition Calculations for Indian Point Unit No.2, Final Report. Environmental Systems Corporation, Knoxville, TN.

Orville, H.D., Hirsch, J.H., May, L.E., 1980. Application of a cloud model to cooling tower plumes and clouds. J. Appl. Meteorol. 19 (11), 1260–1272.

Policastro, A.J., Dunn, W.E., Gavin, P, Boughton, B., Ziebarth, J., 1981a. Studies on Mathematical Models for Characterizing Plume and Drift Behavior from Cooling Towers, Volume 3: Mathematical Model for Single Source (Single-Tower) Cooling Tower Drift Dispersion. CS-1683-V3, Research Project 906–1, Argonne National Laboratory, prepared for Electric Power Research Institute, Palo Alto, CA.

Policastro, A.J., Dunn, W.E., Breig, M., Haake, K., 1981b. Studies on Mathematical Models for Characterizing Plume and drift Behavior from Cooling Towers, Volume 5: Mathematical Model for Multiple Source (MultipleTower) Cooling Tower Drift Dispersion, CS-1683-V5, Research Project 906-1, Argonne National Laboratory, prepared for Electric Power Research Institute, Palo Alto, CA.

Policastro, A.J., Coke, L., Wastag, M., 1984. User's Manual: Cooling-Tower-Plume Prediction Code, Report No. CS-3403-CCM. Electric Power Research Institute, Palo Alto, CA.

Policastro, A.J., Dunn, W.E., Carhart, R.A., 1994. A model for seasonal and annual cooling tower impacts. Atmos. Environ. 28 (3), 379–395. http://dx.doi.org/10.1016/1352-2310(94)90118-X.

Ruiz, J., Cutillas, C.G., Kaiser, A.S., Ballesta, M., Zamora, B., Lucas, M., 2016. Experimental study of drift deposition from mechanical draft cooling towers in urban environments. Energy Build. 125, 181–195. http://dx.doi.org/10.1016/j.enbuild.2016.04.076.

Smith, A., Lott, N., Vose, R., 2011. The integrated surface database: recent developments and partnerships. Bull. Am. Meteorol. Soc. 92 (6), 704–708. http://dx.doi.org/10.1175/2011BAMS3015.1.

U.S. EPA, 2004. User's Guide for the AERMOD Meteorological Preprocessor (AERMET), Publication No. EPA-454/B-03-002. United States Environmental Protection Agency (EPA), Research Triangle Park, NC. https://www3.epa.gov/ttn/scram/metobsdata_procaccprogs.htm#aermet.

U.S. EPA, 2005. Revision to the Guideline on Air Quality Models: Adoption of a Preferred General Purpose (Flat and Complex Terrain), Federal Register 70(216), 68218-68261. U.S. Environmental Protection Agency (EPA), Research Triangle Park, NC. https://www3.epa.gov/scram001/guidance/guide/appw_05.pdf.

U.S. NRC, 2007. Environmental Standard Review Plan Main Report, NUREG-1555, vol. 2 U.S. Nuclear Regulatory Commission, Washington, DC. https://www.nrc.gov/docs/ML0037/ML003701937.pdf.

U.S. NRC, 2008. Final Environmental Impact Statement for an Early Site Permit (ESP) at the Vogtle Electric Generating Plant Site Final Report, NUREG-1872. U.S. Nuclear Regulatory Commission, Washington, DC. https://www.nrc.gov/reading-rm/doc-collections/nuregs/staff/sr1872/.

U.S. NRC, 2011. Detroit Edison Fermi 3 COLA Environmental Report (Rev.3) Chapter 5

Environmental Impacts of Operation, NRC ML110600491. U.S. Nuclear Regulatory Commission, Washington, DC. https://www.nrc.gov/docs/ML1106/ML110600491.pdf.

U.S. NRC, 2013. Comanche Peak Nuclear Power Plant, Unit 3 & 4 COL Application Part 3-Environmental Report (Rev.4) Chapter 5 Environmental Impacts of Operation, NRC ML13345A663. U.S. Nuclear Regulatory Commission, Washington, DC. https://www.nrc.gov/docs/ML1334/ML13345A663.pdf

U.S. NRC, 2014a. APR1400 Design Control Document Tier 2 Chapter 9 Auxiliary Systems (Rev.0), NRC ML15006A048. U.S. Nuclear Regulatory Commission, Washington, DC. https://www.nrc.gov/docs/ML1500/ML15006A048.pdf.

U.S. NRC, 2014b. APR1400 Design Control Document Tier 2 Chapter 10 Steam and Power Conversion System (Rev.0). NRC ML15006A049. U.S. Nuclear Regulatory

Commission, Washington, DC. https://www.nrc.gov/docs/ML1500/ML15006A049.pdf.

U.S. NRC, 2014c. APR1400 Design Control Document Tier 2 Chapter 2 Site Characteristics (Rev.0), NRC ML15006A041. U.S. Nuclear Regulatory Commission, Washington, DC. https://www.nrc.gov/docs/ML1500/ML15006A041.pdf.

U.S. NRC, 2015. Ultimate Heat Sink for Nuclear Power Plants, NRC RG 1.27. U.S. Nuclear Regulatory Commission, Washington, DC. https://www.nrc.gov/docs/ML1410/ML14107A411.pdf.

Wan, P.K., 2007. Atmospheric dispersion analysis in preparing permit applications for the new nuclear power plants in the United States. In: Proceedings of 15th International Conference on Nuclear Engineering (ICONE), Session ID ICONE15–10658, Nagoya, Japan. doi: 10.1299/jsmeicone.2007.15._ICONE1510_360.